Interannual fluctuations in the seasonal cycle of nitrous oxide and chlorofluorocarbons due to the Brewer-Dobson circulation

P. G. Simmonds,[1] A. J. Manning,[2] M. Athanassiadou,[2] A. A. Scaife,[2] R. G. Derwent,[3] S. O'Doherty,[1] C. M. Harth,[4] R. F. Weiss,[4] G. S. Dutton,[5,6] B. D. Hall,[6] C. Sweeney,[5,6] and J. W. Elkins[6]

Received 22 February 2013; revised 4 September 2013; accepted 10 September 2013; published 1 October 2013.

[1] The tropospheric seasonal cycles of N_2O, CFC-11 (CCl_3F), and CFC-12 (CCl_2F_2) are influenced by atmospheric dynamics. The interannually varying summertime minima in mole fractions of these trace gases have been attributed to interannual variations in mixing of stratospheric air (depleted in CFCs and N_2O) with tropospheric air with a few months lag. The amount of wave activity that drives the stratospheric circulation and influences the winter stratospheric jet and subsequent mass transport across the tropopause appears to be the primary cause of this interannual variability. We relate the observed seasonal minima of species at three Northern Hemisphere sites (Mace Head, Ireland; Trinidad Head, U.S.; and Barrow, Alaska) with the behavior of the winter stratospheric jet. As a result, a good correlation is obtained between zonal winds in winter at 10 hPa, 58°N–68°N, and the detrended seasonal minima in the stratosphere-influenced tracers. For these three tracers, individual Pearson correlation coefficients (r) between 0.51 and 0.71 were found, with overall correlations of between 0.67 and 0.77 when "composite species" were considered. Finally, we note that the long-term observations of CFCs and N_2O in the troposphere provide an independent monitoring method complementary to satellite data. Furthermore, they could provide a useful observational measure of the strength of stratosphere-troposphere exchange and, thus, could be used to monitor any long-term trend in the Brewer-Dobson circulation which is predicted by climate models to increase over the coming decades.

Citation: Simmonds, P. G., et al. (2013), Interannual fluctuations in the seasonal cycle of nitrous oxide and chlorofluorocarbons due to the Brewer-Dobson circulation, *J. Geophys. Res. Atmos.*, *118*, 10,694–10,706, doi:10.1002/jgrd.50832.

1. Introduction

[2] The seasonal cycles of long-lived trace gases, such as nitrous oxide (N_2O) and various chlorofluorocarbons (CFCs), are significantly influenced by dynamical transport processes [*Liang et al*., 2008; *Douglass et al*., 2008; *Ishijima et al*., 2010; *Nevison et al*., 2011], particularly stratospheric-tropospheric exchange (STE), which is considered here to include both stratosphere-troposphere transport and troposphere-stratosphere transport [*Bourqui*, 2004]. For these trace gases which are destroyed primarily in the stratosphere (henceforth referred to as stratospheric tracers), the depth of the observed annually varying summertime minima has been attributed to the transport and mixing of stratospheric air, depleted in these tracers, with tropospheric air with a lag time of 3–4 months [*Liao et al*., 2004; *Nevison et al*., 2004, 2007, 2011; *Jiang et al*., 2007]. In addition to the STE influence, there is a contribution to the seasonal cycle of N_2O arising from its seasonally varying surface sources [*Nevison et al*., 2007, 2011; *Huang et al*., 2008]. The complex seasonal cycle in the Southern Hemisphere is more difficult to reconcile with seasonal variations in surface sources and stratospheric intrusions as there are larger modeling uncertainties there [*Prinn et al*., 2000; *Liao et al*., 2004; *Huang et al*., 2008; *Nevison et al*., 2011].

[3] By mass conservation, the wintertime descent of stratospheric air in the extratropics, due to the Brewer-Dobson circulation (BDC), is balanced by the upward transport of tropospheric air in the tropics in a ~40° latitudinal belt (20°S–20°N) [*Wernli and Bourqui*, 2002]. The maximum STE occurs in late winter/early spring, primarily in the midlatitudes (30°–70°N) and accounts for 67–81% of the annual input of air of stratospheric origin into the Northern Hemisphere (NH) extratropical troposphere [*Liang et al*., 2009]. Given the strong gradient in stratospheric tracers between air entering and leaving the stratosphere, depletion of such tracers is sensitive to the amount of stratosphere-troposphere transport.

[1]Atmospheric Chemistry Research Group, University of Bristol, Bristol, UK.
[2]Met Office, Exeter, UK.
[3]rdscientific, Newbury, UK.
[4]Scripps Institution of Oceanography, University of California, San Diego, La Jolla, California, USA.
[5]Cooperative Institute for Research in Environmental Sciences, University of Colorado, Boulder, Colorado, USA.
[6]NOAA Earth System Research Laboratory, Boulder, Colorado, USA.

Corresponding author: P. G. Simmonds, Atmospheric Chemistry Research Group, University of Bristol, Bristol BS8 1TH, UK. (petergsimmonds@aol.com)

2169-897X/13/10.1002/jgrd.50832

[4] The BDC is driven by vertically propagating Rossby and gravity waves in the stratosphere and the lower mesosphere at heights between 15 and 60 km. The breaking of these waves drive a net zonal westward force on the atmosphere at the height of the wave breaking, a deceleration of the dominant eastward winds at that level, and the meridional circulation. This deceleration of the jet drives the meridional circulation in the stratosphere and, hence, high-latitude convergence and the descent of stratospheric air into the troposphere. The Rossby wave activity varies from year to year, with years when the breaking is stronger causing greater deceleration of the jet, more vertical transport, and, consequently, a greater degree of STE. Various model simulations of the impact of increasing greenhouse gases on climate predict strengthening of the BDC, which, in turn, suggests an increase in the transport of stratospheric air into the troposphere [*Butchart and Scaife*, 2001; *Butchart et al*., 2006; *Garcia and Randel*, 2008, and references therein; *Liang et al*., 2008].

[5] *Nevison et al*. [2011] reported a strong anticorrelation between the residuals derived from the detrended monthly means of N_2O and the mean polar (60°–90°) lower stratospheric (100 hPa) temperature in winter/spring in both hemispheres. The stratospheric temperature was serving as a proxy for STE in their study. The amount of wave activity driving the stratospheric jet behavior and, subsequently, the mass transport across the tropopause was thus reported to be the primary cause of interannual variability in tropospheric N_2O, CFC-11, and CFC-12 mixing ratios.

[6] In section 2 of this paper, we describe the methods used for tracer species measurements and analysis. Section 3 describes the meteorological analysis. We confirm in section 4 that the observed variations in tracer mixing ratios are in approximate quantitative agreement with the values expected from year-to-year fluctuations in STE. Results and discussion in section 5 explore the relationship between the magnitude of the summertime minima of N_2O, CFC-11, and CFC-12 mixing ratios at the surface and the variation of the STE. In section 5.3, we provide a limited examination of aircraft measurements of tracer vertical profiles [NOAA's Carbon Cycle and Greenhouse Gas Group's (CCGG) Aircraft program; www.esrl.noaa.gov/gmd/ccgg/aircraft/] to establish if there is a link between STE and the lowermost troposphere. In section 6, we briefly examine other modes of atmospheric circulation that might be expected to influence the seasonality of stratospheric tracers, and the conclusions are in section 7. In section 8, we propose potential applications of our results.

[7] Finally, from the Mace Head Atmospheric Research Station (MHD), we propose a "composite" (mean of N_2O, CFC-11, and CFC-12) tracer value whose seasonal variation can be used as a good proxy measure of the strength of STE and, hence, the Brewer-Dobson circulation.

2. Methods (Measurements and Analysis)

2.1. Mace Head, Ireland (53.3°N, 9.9°W)

[8] MHD is located in Connemara, Co. Galway, on the Atlantic Ocean coastline of Ireland and is operated as part of the Advanced Global Atmospheric Gases Experiment (AGAGE), a network of globally distributed observing sites. MHD offers a "clean" sector from 180° to 300° (~S through WNW) not affected by recent emissions. Meteorological records show that on average, over 70% of the air masses arrive at the site in the clean air sector. Air is sampled at a height of 14 m above sea level from a tower situated 90 m from the shoreline and 50 m from high water. The area around MHD is generally wet and boggy with exposed rock. The soil type is peat with a depth that varies from a few centimeters on hill slopes to a few meters on flatter grounds. There are few trees, with the vegetation consisting mainly of grasses, sedges, ferns, rushes, gorse, and heathers (http://macehead.org).

[9] N_2O, CFC-11, and CFC-12 measurements are recorded every 20 min using an automated custom-built gas chromatograph coupled with twin electron capture detectors with a standard calibration and ambient air analysis alternated 36 times throughout each day. By averaging the two bracketing calibrations, this provides a calibrated measurement every 40 min. Data were selected from 1995 to 2010 to coincide with the introduction of improved higher-precision instrumentation, particularly for N_2O, as part of the transition from Global Atmospheric Gases Experiment to AGAGE [*Prinn et al*., 2000]. All AGAGE data are reported on the Scripps Institution of Oceanography 2005 calibration scale.

2.2. Trinidad Head, U.S. (40°N, 124.2°E)

[10] We examine CFC-11 and CFC-12 baseline-selected observations recorded at Trinidad Head (THD) located on the west coast of California, which is also part of the AGAGE network and employs the same instrumentation and calibration methodology as MHD. Although we include observations of N_2O, we note that the seasonal cycle of N_2O at THD is sometimes influenced by summertime coastal upwelling [*Lueker et al*., 2003].

2.3. Point Barrow, Alaska (71.3°N, 156.6°W)

[11] Point Barrow (BRW) is one of the observing sites of the National Oceanic and Atmospheric Administration/Earth System Research Laboratory/Global Monitoring Division (NOAA/ESRL/GMD; http://www.esrl.noaa.gov/gmd) and records CFC and N_2O mixing ratios through in situ measurements, typically once an hour, using the Chromatograph for Atmospheric Trace Species (CATS) [*Hall et al*., 2007]. Data for these species are also collected every ~1–2 weeks as part of a flask sampling program (NOAA/HATS). Flask and in situ data, where available, are combined into a single data set referred to as "NOAA/HATS Combined". In this investigation, we explore both NOAA in situ CATS and NOAA/HATS Combined (HATS), which are statistically filtered to remove pollution events [*Hall et al*., 2011]. The current calibration scales are CFC-11 (NOAA-1993), CFC-12 (NOAA-2008), and N_2O (NOAA-2006A; http://www.esrl.noaa.gov/gmd/ccl/n2o_scale.html). The ratio of NOAA/AGAGE for N_2O is 0.9999 ± 0.0010 with slight time dependence; for CFC-12, the ratio is 0.9966 ± 0.0011 with good consistency. For CFC-11, the ratio is time dependent (2002–2012, standard deviation is 0.3–0.4%); however, it is not necessary to adjust the numbers to a common calibration scale when analyzing seasonal variations relative to the long-term trend at the same site.

2.4. Baseline Mass Mixing Ratios

[12] The MHD monthly mean baseline mixing ratios of N_2O, CFC-11, and CFC-12 are calculated from the long-term observational record of trace gas measurements. Baseline mixing ratios are defined here as those that have not been

influenced by significant anthropogenic or local emissions within the past 30 days of travel to MHD, i.e., those that are well mixed and are representative of the midlatitude Northern Hemisphere background concentrations. Baseline mixing ratios are calculated for each hour by interpolating, using a quadratic best fit function, within a moving time window from all measurements recorded when the air is classified as "baseline". Points are defined as baseline or not, through the use of air history maps calculated using the Numerical Atmospheric dispersion Modeling Environment model. The process selects only those measurements that have a small local footprint (the contribution from the nine grid cells centered on MHD is low), a minimal contribution from populated areas, and a minimal contribution from southerly latitudes. Using MHD N_2O observations, the method defines ~47% of them as baseline, significantly less than what might be expected from the clean air sector due to the removal of local and southerly influences. Full details of the method for calculating atmospheric baselines from remote surface sites are described in *Manning et al*. [2011].

[13] Work has been undertaken to understand the uncertainty in estimating the baseline trends, growth rates, and seasonal cycles. Working with the estimated hourly baseline values, the time series is split into two separate components, namely, a long-term trend and a seasonal variability component. Three different methods have been explored in order to define the long-term and seasonal variability components and enable an estimation of the uncertainty.

2.4.1. Method 1 (KZ-1year)

[14] A Kolmogorov-Zurbenko (KZ) [*Rao and Zurbenko*, 1994] filter involves a number of iterations of a moving average of a given time duration and is ideally suited to this type of problem. For this application, the length of the moving average window was set to 1 year, and for Method 1, the number of iterations was set to 1. With these parameters, Method 1 is a simple 12 month running average approximately removing wavelengths smaller than 1 year. At each hour in the time series, the 12 month average of the baseline mass mixing ratios centered on this hour is calculated. This is the long-term trend component; subtracting this from the actual hourly baseline estimate at this time gives the seasonal variability.

2.4.2. Method 2 (KZ-2year)

[15] The KZ filter was used again, but for this method, the number of iterations was set to 4, i.e., a 12 month moving average was applied to the data 4 times, thereby approximately removing periods smaller than 2 years.

2.4.3. Method 3 (3yr-quadratic)

[16] At each hour, calculate the 12 month average centered on this hour (y_a). For the 3 year period centered on this hour, calculate the quadratic line using the standard value decomposition that best fits y_a data. This is the long-term trend component; subtracting this from the actual hourly baseline estimate at this time gives the seasonal variability.

2.5. Analysis of Vertical Profile Measurements

[17] We next examine if vertical profile measurements of N_2O and CFC-11 can provide a connection between STE and the lowermost troposphere. Selected vertical profiles for the tracer species were obtained from the small aircraft sampling program of the CCGG group of NOAA/ESRL (http://www.esrl.noaa.gov/gmd) for the following sites: ETL (East Trout lake, Saskatchewan, Canada, 54.4°N, 105.0°W), a remote site in the same midlatitude band of the NH as MHD, and ULB (Ulaanbaatar, Mongolia, 47.4°N, 106°E), with limited data from 2006 to 2008 due to funding constraints to compare with previously recorded vertical profiles [*Ishijima et al*., 2010] from a site in Surgut, West Siberia, Russia (61.3°N, 73.4°E). Vertical profiles recorded at THD were quite sparse in some years, with significant gaps due to the removal of contaminated data; however, we did examine N_2O vertical profiles to observe the potential interference by local sources, especially in summertime during periods of strong coastal upwelling [*Lueker et al*., 2003].

[18] Monthly averages (one to six profiles per month) were calculated from the vertical profile observations and binned into 1000 m altitude bands (0–1 km, 1–2 km, etc.); however, due to limited data at the higher altitudes, we averaged values for the highest 2 km band. Since there are no in situ measurements at either ETL or ULB, we subtracted the THD NOAA/HATS Combined monthly means from the ETL average monthly vertical profiles and MHD NOAA/HATS Combined monthly means from the ULB average monthly vertical profiles, as proxies for the absence of in situ measurements at these sites. These mixing ratio vertical profile anomalies were then compiled into bimonthly summaries and plotted against the individual altitude levels. We accept that the sites selected provide only limited spatial sampling; however, for many other sites, vertical profiles were quite sparse, often with large uncertainties. The detailed analysis of more sites and the absence of in situ observations at any specific site would not have contributed significantly more information and was beyond the scope of this investigation.

[19] We also note that evidence for a Jet-STE-surface link might be possible from satellite data. Recently published CFC-11 and CFC-12 profiles from analysis of data from the Michelson Interferometer for Passive Atmospheric Sounding-Envisat have indicated clear evidence of transport from the stratosphere to the troposphere [*Kellmann et al*., 2012]. Interestingly, the authors noted that CFC trends in the stratosphere vary with altitude and latitude, and in some regions, even positive trends are observed, which, in some cases, could be only explained by changes in atmospheric age of air spectra or vertical mixing patterns. However, at most altitudes and latitudes, negative trends are observed which are, on average, consistent with the trends in tropospheric CFC mixing ratios. In general, the satellite observations do not have sufficient resolution and precision for studying stratospheric tracers in the lowermost troposphere (generally $<$4000 m) [*Kellmann et al*., 2012]. Furthermore, they cannot accurately define the amplitude of the tracer seasonal cycles, which is the strength of the surface-based observing sites with high-frequency, high-precision measurements.

3. Analysis of Meteorological Data

[20] Global monthly means of the Northern Hemisphere winter zonal wind (U) at 10 hPa were retrieved from the ECMWF ERA-Interim data set [*Berrisford et al*., 2009] for the years 1991–2011 at a resolution of 2° × 2°. From these data, Northern Hemisphere winter mean zonally averaged zonal winds were constructed for all NH latitudes. For example, the DJF03 zonal wind average at a given latitude is constructed by averaging the December 2002, January 2003,

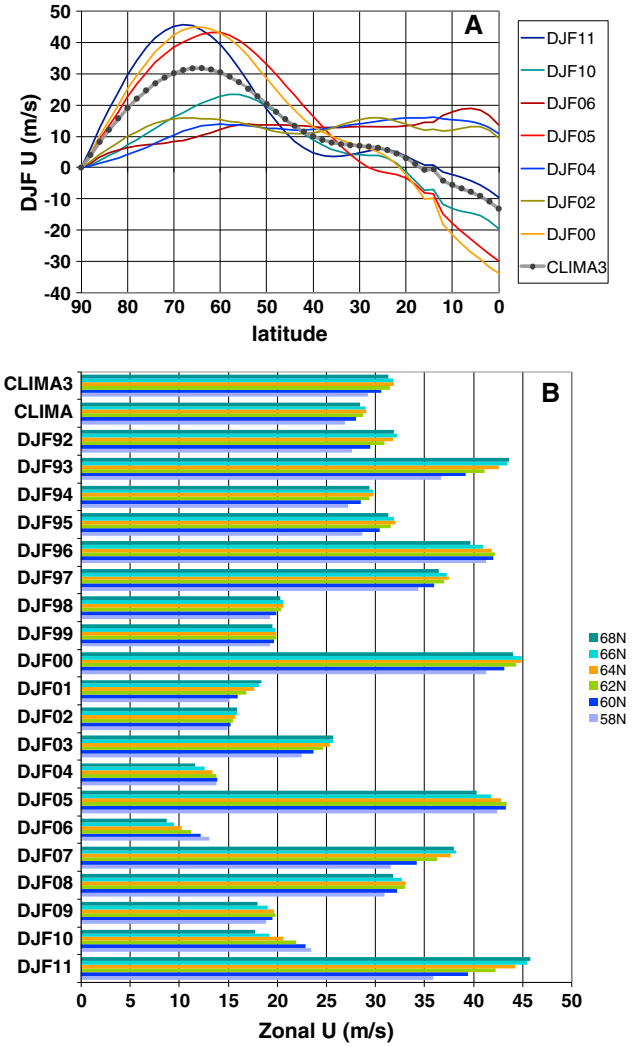

Figure 1. (a) Selected examples of the jet behavior at 10 hPa from 2000 to 2011. "Clima" is the average climatology using all years 1992–2011. (b) Latitudinal variation of the DJF winds in the band from 58°N to 68°N.

and February 2003 10 hPa mean zonal winds for that latitude. A climatological December, January, and February (DJF) mean value is obtained by averaging all 20 DJF values for the years 1992–2011. The deviation from the climatological mean of each DJF at each 2° band (58°N–68°N) was calculated and is used to define the stratospheric jet. The mean zonal easterly winds at 60°N and 10 hPa is the widely used WMO definition of sudden stratospheric warmings and is a strong indication of dynamical coupling. Here we use the deviation of the climatological mean across the latitudinal range from 58°N to 68°N as an estimate of the uncertainty in our wind analysis. Moreover, the median of these values is assumed here to show the behavior of the stratospheric jet in that year and is used in the correlation with the tracer species mixing ratios. Negative deviations from the mean imply a weaker than average jet, a stronger than average downward transport, and, consequently, a greater degree of STE. Figure 1a shows the latitudinal variation of the jet behavior at 10 hPa for selected years with strong and weak jets. Plotted are DJF values of zonal winds averaged at each 2° latitude band in the NH. "Clima" is the average climatology using all years 1992–2011. For example, 2000 and 2005 are typical years with strong jets at around 64°N and, consequently, less STE. Conversely, for the years 2002, 2004, and 2006, the jet is very much reduced and/or moved south. These are years with strong STE when we might expect lower summer minima in the seasonal cycles of the stratospheric tracers. Figure 1b shows the latitudinal variation of the DJF winds in the band from 58°N to 68°N. Except for 1993, 2007, 2010, and 2011, the magnitude of the latitudinal variation is less than 5 m/s.

4. Simple Quantitative Explanation of Observed Tracer Fluctuations

[21] We now estimate the magnitude of typical variations of tropospheric mixing ratios and compare these with interannual fluctuations in the MHD data.

[22] Fluctuations in the mean westerly jet and the associated changes in meridional overturning are highly correlated from year to year because they are driven by the same wave breaking and dissipation in the middle atmosphere [*Andrews and McIntyre*, 1978]. Assuming all of the resulting upward mass flux occurring in a "tropical pipe" is balanced by equal and opposite downward fluxes into the extratropical troposphere [*Holton et al.*, 1995], we can estimate an idealized mass flux based on lower stratospheric vertical residual velocities [*Andrews and McIntyre*, 1978]. Using typical interannual fluctuations in the upwelling velocities, we can then estimate the % fluctuation in the tropospheric mass mixing ratios of the tracers. Figure 2 shows this process schematically.

[23] The rate of upwelling mass M passing through the tropopause is given by

$$dM/dt = \rho_T W^* f A \quad (1)$$

[24] where ρ_T is the density of air at the tropical tropopause, W^* is the density averaged residual vertical velocity in the tropical upwelling region, f is the proportion of the globe in the upwelling region, and A is the surface area of the Earth.

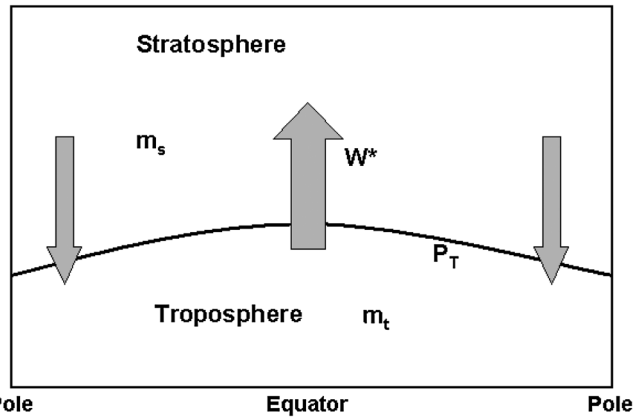

Figure 2. Schematic representation of an idealized mass budget between tropical upward mass flux and equal and opposite downward fluxes into the extratropical troposphere.

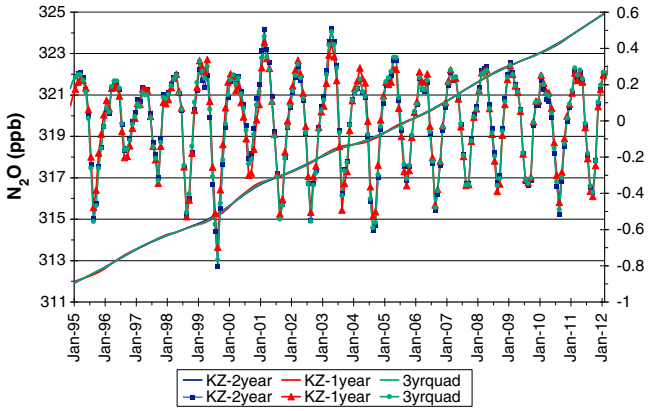

Figure 3. Mass mixing ratio trend lines for the Mace Head N_2O from the application of the three detrending methods (left-hand axis) and estimated seasonal variability mass mixing ratios for each method (right-hand axis).

[25] The mass m_t of the troposphere can be approximated (assuming hydrostatic balance) as

$$m_t = (A/g)\cdot(P_o - P_T) \tag{2}$$

[26] where g is gravity; and P_T and P_o are the pressure at the tropopause and the surface, respectively.

[27] From (5) and (6), the fractional rate of tropospheric mass exchanged with the stratosphere F can be obtained from

$$dF/dt = (\rho_T g\, W^* f)/(P_o - P_T) \tag{3}$$

[28] If we now consider W^* as a typical interannual variation in the upwelling velocity, then an estimate of a typical fluctuation in the troposphere-stratosphere mass exchange can be made. We use typical values of $\rho_T \sim 0.1$ kg m^{-3}, $g \sim 10$ ms^{-2}, $f \sim 0.3$, $dt \sim 1.6 \times 10^7$s (assuming active transport for around 6 months in the winter half year), $P_o = 10^5$ Pa, and $P_T = 10^4$ Pa. We estimate W^* as 0.1 m ms^{-1} based on typical year-to-year variability seen in general circulation models in the lower stratosphere [*Scaife et al.*, 2002].

[29] This gives a typical year-to-year fluctuation (F) of 0.005 or about 0.5% of the tropospheric air. Assuming a well-mixed troposphere with mean mass mixing ratios of 320 ppb, 540 ppt, and 250 ppt for N_2O, CFC-12, and CFC-11, respectively, and complete depletion of the tracers in the stratosphere, this simple theory suggests typical year-to-year fluctuations of around 1–2 ppb, 2–3 ppt, and 1–2 ppt for N_2O, CFC-12, and CFC-11, respectively. These numbers are similar in magnitude to the year-to-year fluctuations observed, namely, 0.6 ppb, 1.2 ppt, and 0.9 ppt, respectively. Given that chemical depletion in the stratosphere is also unlikely to be complete, the consistency between these estimates confirms that the year-to-year fluctuations in surface tropospheric mixing ratios of the stratospheric tracers are likely to be strongly affected by year-to-year fluctuations in stratosphere-troposphere mass exchange.

5. Results and Discussion

5.1. Seasonal Variability of the Tracer Species at Mace Head, Ireland

[30] Figure 3 illustrates the mass mixing ratio trend lines for MHD N_2O from the application of the three detrending methods and the estimated seasonal variability mass mixing ratio for each method. While the trends determined by each method are in close agreement, it is clear that the seasonal variability derived from each detrending method does have small but significant differences. Figure 4a shows monthly means of seasonal variability (average of the three detrending methods) for CFC-11, CFC-12, and N_2O, from 1995 to 2011, where CFC-11 and CFC-12 were normalized to N_2O units by multiplying by the ratio of the mean tropospheric mixing ratio $x(N_2O)/x(CFC)$, where $x(N_2O)$ is in ppb and $x(CFC)$ is in ppt. Although the maximum STE is expected during the winter months, the greatest impact, i.e., in the minima of the species mixing ratios at the surface, is observed in the summer months from June through September due to the several months lag time for the transport of stratospheric air down to the lower troposphere and subsequent mixing [*Nevison et al.*, 2004; *Liang et al.*, 2009]. The spring 1996 and 1997 minima in CFC-12 are notably out-of-phase with the other two tracers. In both of these years, there is a positive deviation of the wind relative to the climatological mean, implying no significant deceleration of the jet. Therefore,

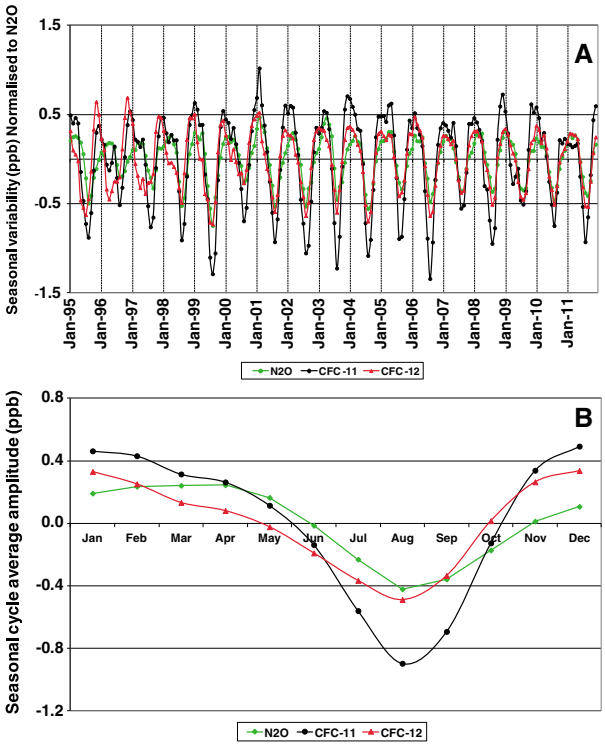

Figure 4. (a) Means of seasonal cycle variability for CFC-11, CFC-12, and N_2O, from 1995 to 2011, where CFC-11 and CFC-12 were normalized to N_2O units by multiplying by the annual baseline mean tropospheric mixing ratio of N_2O/CFC, where N_2O is in ppb and CFC is in ppt. (b) Climatological average (1995–2011) seasonal cycle for each species. As in Figure 4a, CFC-11 and CFC-12 are normalized to N_2O units (ppb).

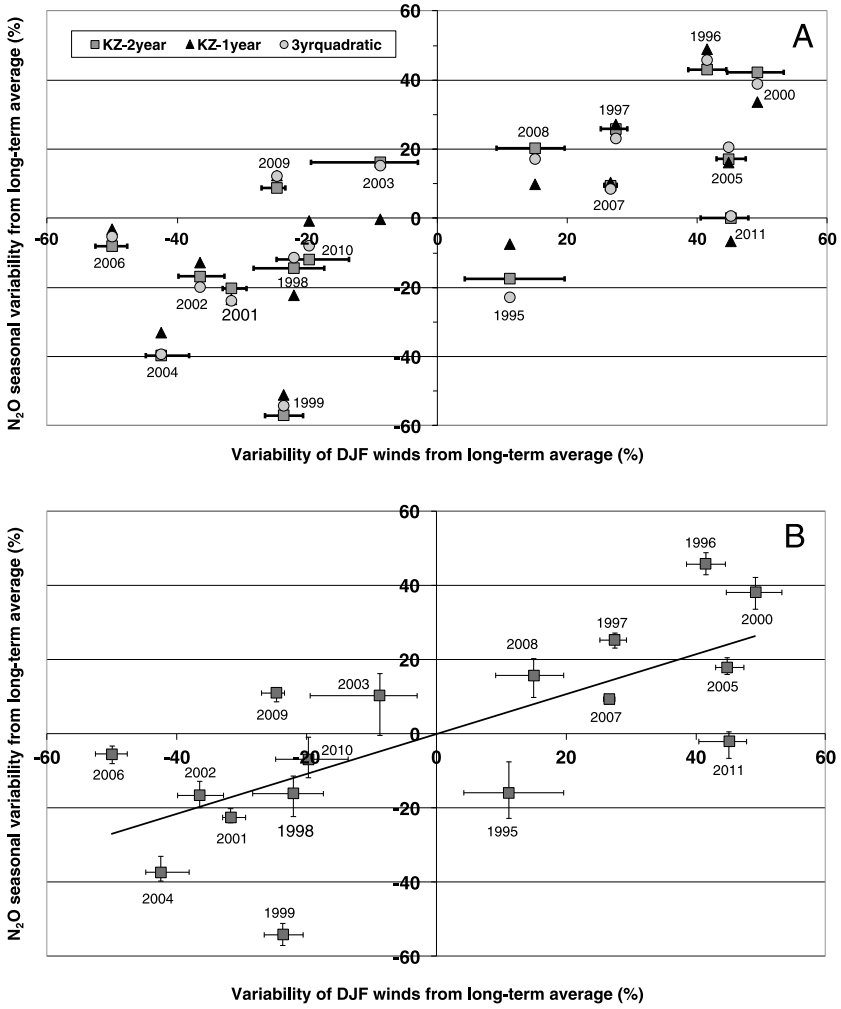

Figure 5. (a) Scatterplot of the % seasonal variability of N_2O from the long-term average of N_2O at MHD using three detrending methods versus the % variability of the winds. The uncertainty, over the 58°N–68°N latitude band, of the % variability of the winds is applicable to all three methods but, for clarity, is only added to the KZ-2year points. (b) Scatterplot of the seasonal variability of N_2O from the average of the three detrending methods, including the uncertainty versus the % variability of the winds with uncertainty.

strong STE is unlikely to have occurred, and the seasonal variations in CFC-12 mixing ratios will be largely dominated by tropospheric transport and sources, with CFC-12 still growing at an annual average rate of 3–4 ppt/yr during 1996–1997.

[31] As noted by *Nevison et al*. [2004], the degree of depletion should be proportional to the atmospheric lifetime, where CFC-11 with the shortest lifetime (45–52 years) has the lowest summertime minimum in the seasonal amplitude. It was also noted that CFC-12 leads the other stratospheric tracers by about 1 month. Our data confirm this observation, at least in the early part of the record; however, the time lag in CFC-12 gradually disappears, so that after about 2000, the CFC-12 minima are in August and are in phase with the other two tracers. Interestingly, this period coincides with the transition when the tropospheric mixing ratio of CFC-12 maximizes and then begins to decline. *Liang et al*. [2008] suggested from a model simulation that this time lag in CFC-12 may be associated with changes in the distribution of regional emissions in the 1990s because of rapid decreases in emissions in North America and Europe. Figure 4b shows that the climatological average (1995–2011) seasonal cycle for each species, as in Figure 4a CFC-11 and CFC-12, were normalized to N_2O units (ppb).

5.2. Relationship With Circulation

[32] As discussed in the introduction, the strength of the stratospheric meridional circulation and, therefore, STE mixing is associated with the behavior of the upper stratospheric jet (and variations in Rossby wave activity). So we correlated the species' seasonal variability at the surface with the jet's behavior. As a measure of the stratospheric jet, we use the wintertime zonal winds (averaging the December, January, and February winds) at 10 hPa and 58°N–68°N, expecting that these will provide a robust predictor of the depth of the surface summertime minima in the seasonal cycles of the stratospheric tracers.

[33] Figure 5a compares the % variation of the seasonal variability from the long-term average of N_2O at MHD for each detrending method (KZ-1year, KZ-2year, and 3yr-quadratic)

Table 1. Correlations Between the Variability of the (% Deviation From the Average) DJF 10 hPa Winds in the 58°N–68°N Latitude Band and the Mean Tracer Seasonal Variability (% Deviation From the Average) of the Three Detrending Methods From 1995 to 2011 at MHD, THD, and BRW[a]

Station/Tracer Species	Latitude, Longitude Network	Time Series	Significance Level of Mean Correlation (%)
Mace Head, Ireland (MHD)	53.33°N, 9.9°W	1995–2011	
N_2O	AGAGE	0.71 (0.69–0.72)	99.9
CFC-11	AGAGE	0.55 (0.50–0.59).	97.8
CFC-12	AGAGE	0.63 (0.59–0.65)	99.3
Composite Tracer[b]	AGAGE	0.68 (0.65–0.69)	99.7
Trinidad Head, U.S. (THD)	41.05°N, 124.15°E	1996–2011	
N_2O[c]	AGAGE	0.41[c] (0.37–0.43)	88.5
CFC-11	AGAGE	0.69 (0.60–0.73)	99.7
CFC-12	AGAGE	0.59 (0.56–0.60)	98.4
Composite Tracer[d]		0.78 (0.75–0.79)	99.9
Barrow, Alaska (BRW)	71.32°N, 156.61°E	1995–2011	
N_2O	NOAA (HATS)	0.15 (0.01–0.25)	43.5
CFC-11	NOAA (HATS)	0.42 (0.37–0.43)	90.7
CFC-12	NOAA (HATS)	0.26 (0.13–0.33)	68.7
Barrow, Alaska (BRW)	71.32°N, 156.61°E	1999–2011	
N_2O	NOAA (CATS)	0.53 (0.42–0.60)	93.8
CFC-11	NOAA (CATS)	0.68 (0.62–0.71)	99.0
CFC-12	NOAA (CATS)	0.51 (0.40–0.59)	92.5
Composite Tracer[b]		0.67 (0.64–0.71)	98.8

[a]The range in brackets shows the uncertainty in the correlation when the different methods are used individually.
[b]Mean N_2O, CFC-11, and CFC-12 seasonal variability.
[c]Seasonal cycle potentially influenced by summertime coastal upwelling.
[d]Mean CFC-11 and CFC-12 seasonal variability. When N_2O is included in the composite $r = 0.77$. (HATS) = NOAA/HATS Combined.

with the % variability of the DJF winds, including uncertainty over the 58°N–68°N latitude band. In Figure 5b, we average the seasonal variability for N_2O from the three detrending methods, including the uncertainty over the three methods, versus the % variability of the winds as in Figure 5a. Overall, there is a good correlation between the tracer seasonal variability and the winds; however, this relationship is weaker in some years and notably anticorrelated during 1995, 2003, 2009, and 2011. The winter of 2009/2010 had a very weak polar vortex and exceptionally negative North Atlantic Oscillation (NAO) [*Fereday et al*., 2012]; furthermore, there were reemerging ocean temperature anomalies in late 2010 associated with a repeat negative NAO [*Taws et al*., 2011]. Winter 2010/2011 also showed unusual circulation patterns (A. Maidens, et al., Predictability of the North Atlantic Oscillation in early winter 2010/11, submitted to *Monthly Weather Review*, 2013). There also appears to be some evidence for a recent shift in the position of the polar jet that might be expected to enhance the interannual variability of the stratospheric circulation [*Mizuta*, 2012]. Clearly, there are several interconnected and competing influences affecting these correlations, for example, both the El Niño and the easterly phase of the quasi-biennial oscillation (QBO) are associated with a warmer polar stratosphere in winter [*Garfinkel and Hartmann*, 2007].

[34] Table 1 summarizes the Pearson correlation coefficient (r) for the individual tracers at MHD and the winds during 1995–2011. For the years when the stratospheric jet is strongly decelerated (relative to the climatological mean), we observe deeper summertime minima (relative to the mean) in the species mixing ratios. The average individual correlation coefficients (r) (1995–2011) at MHD for N_2O, CFC-11, and CFC-12 were 0.71, 0.55, and 0.63, respectively, with stronger winds corresponding to higher tropospheric tracer concentrations as expected. All three correlation coefficients are significant at the 95% confidence level. It is noteworthy that over the shorter time frame of 1995–2008, correlations were 0.80 (N_2O), 0.76 (CFC-11), and 0.74 (CFC-12), in close agreement with previous reports [*Nevison et al*., 2004, 2011].

[35] We next create an artificial new composite tracer by averaging the seasonal variability of the three tracers at MHD, and in Figure 6, we relate this composite tracer to the winds. We observe good correlations between the composite and the strength of the deviations of the previous wintertime (DJF) stratospheric winds in 13 of the 17 years of observations. In 1995, 1998, 2009, and 2010, the composite tracer and the winds are anticorrelated. Correlations of this composite tracer with the winds, as shown in Figure 6, are 0.68 (1995–2011) and 0.82 (1995–2008). The years that show the largest summer minima for the composite tracer were 1999, 2001, 2002, 2004, and 2006, while 2003 also has a significant minimum. This implies that a weak stratospheric jet and the resulting enhanced vertical transport leads to greater STE and, thus, lower summer minima in the seasonal cycles of all of the stratospheric tracers. *Manney et al*. [2005, 2008] reported that the years with the most intense recent warming in the Arctic were observed in 2004 and 2006/2007 and, most recently, in the winter of 2009 [*Manney et al*., 2009; *Di Biagio et al*., 2010]. Where the mean zonal winds have a large positive deviation from the 20 year average (1996, 1997, 2000, 2005, 2007, and 2008), the tracer seasonal variability also shows strong positive deviations, i.e., smaller summer minima. As noted previously, there are other factors that cause climate variability in both the stratosphere and the troposphere, in addition to the stratospheric winds which will influence the depth of the tracer summertime minima. We would not therefore expect to see a perfect correlation in all years.

[36] We also include in Figures 7a and 7b and Table 1 similar correlations of the composite tracer with the winds for THD and BRW (CATS and NOAA/HATS Combined data sets),

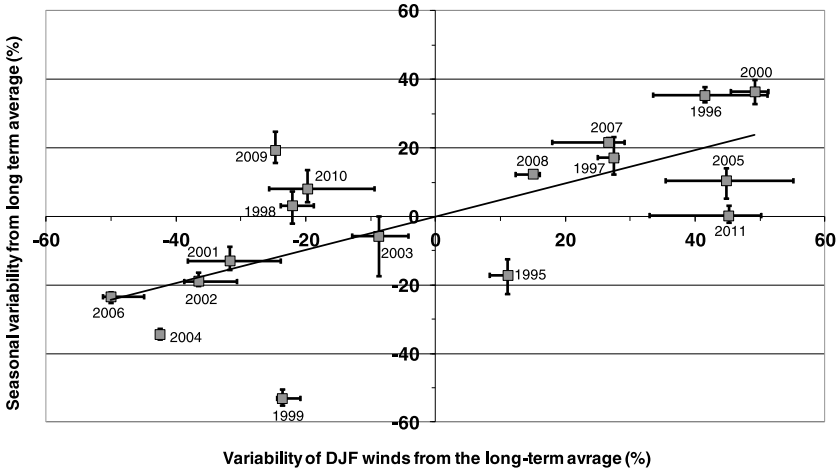

Figure 6. Scatterplot with the linear trend line of the composite tracer (mean of N_2O, CFC-11, and CFC-12 at MHD) by the three detrending methods, including the uncertainty versus the % variability of the winds with uncertainty.

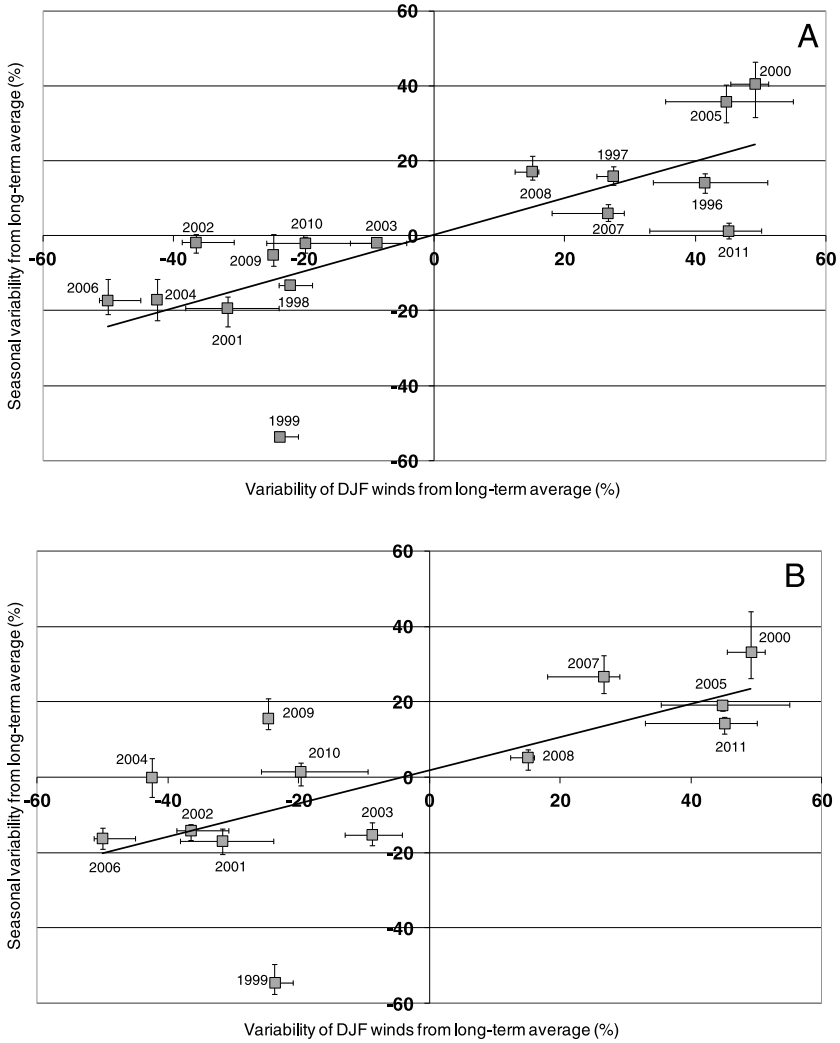

Figure 7. (a) Scatterplot with the linear trend line of THD composite tracer (mean of CFC-11 and CFC-12) versus the % variability of the winds with uncertainty. (b) Scatterplot with the linear trend of BRW CATS composite tracer (mean of N_2O, CFC-11, and CFC-12) versus the % variability of the winds with uncertainty. The composite is the mean of the three detrending methods as described in the text.

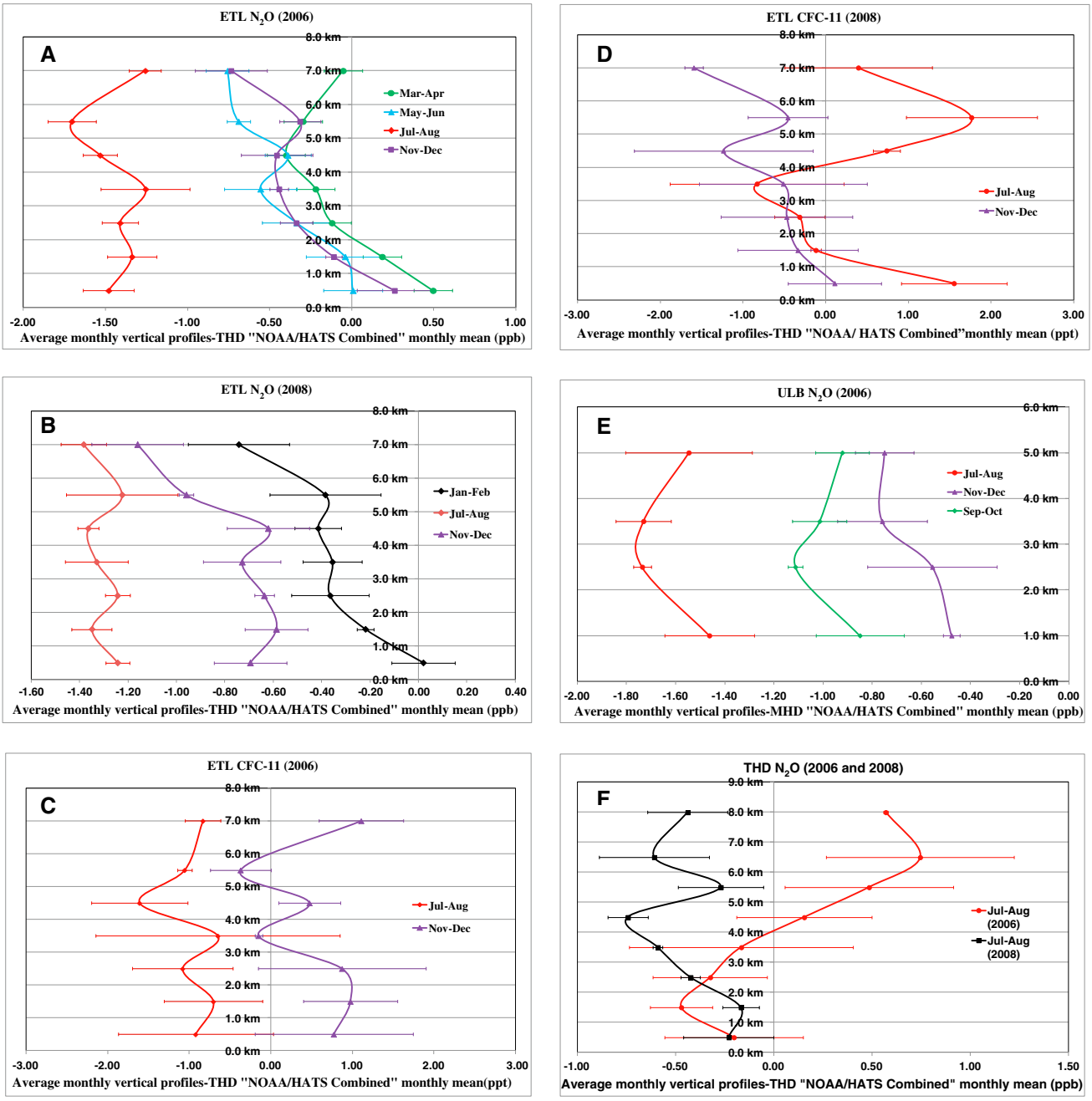

Figure 8. Mixing ratio vertical profile anomalies for N_2O and CFC-11 at (a–d) ETL, (e) ULB, and (f) THD. (Error bars are 1σ standard deviation.) Data were provide by B. Miller, C. Sweeney, and S. Montzka through ongoing work at NOAA and Cooperative Institute for Research in Environmental Sciences.

using the same three detrending methods as employed at MHD. Note that at THD, where overall species correlations are generally good, the composite only includes CFC-11 and CFC-12 with a high correlation of 0.78. We initially excluded N_2O at THD due to the potential ocean upwelling; however, including N_2O in the composite yields a similar correlation of 0.77, suggesting that the influence of N_2O upwelling may be quite small. Interestingly, at THD, there is a good correlation between the winds and the seasonal variability during 2009–2010, which was not the case at MHD. BRW correlations using the NOAA/HATS Combined data are notably weaker (43.5–90.7% level of significance) than the in situ CATS data (92.5–99.0% level of significance) (see Table 1). This may be partly due to the lower-frequency flask data incorporated into the NOAA/HATS Combined data set, but other factors, including local sources and variations in tropospheric transport, could be also important. It is generally accepted that detecting the small amplitudes of these tracer seasonal cycles is more difficult when using data from a ~1 to 2 week flask sampling program compared with the much higher frequency of in situ measurements [*Liang et al.*, 2009; *Nevison et al.*, 2011]. It is noteworthy at BRW that the seasonal variability

Table 2. Correlations Between the Mean Tracer Seasonal Variability (% Deviation From the Average) of the Three Detrending Methods for N_2O, CFC-11, and CFC-12 and the NAO and ENSO Indices

Tracer	ENSO[a] (1995–2011)	NAO[b] (1995–2011)
N_2O	0.18	0.0
CFC-11	0.004	0.22
CFC-12	0.08	0.09

[a]www.cpc.ncep.noaa.gov.
[b]www.cgd.ucar.edu/cas/hurrell/indices.html.

in 2009 and 2010 are anticorrelated with the winds (see MHD) but correlated during 2011.

[37] Tracer-tracer correlations of the mean of the August seasonal variability from 1996 to 2011 (month of the largest summertime minima) determined from the KZ-2year detrending method reveal robust correlations. For example, at MHD, N_2O versus CFC-12 has $r=0.89$, N_2O versus CFC-11 has $r=0.78$, and CFC-11 versus CFC-12 has $r=0.78$. Similarly, at THD, N_2O versus CFC-12 has $r=0.72$, N_2O versus CFC-11 has $r=0.56$, and CFC-11 versus CFC-12 has $r=0.70$. This suggests that our baseline selection process effectively removes any major contribution from terrestrial sources to the seasonal tropospheric boundary layer mixing ratios of the tracers. However, this is not conclusive, and there could remain some small influences from seasonal coastal marine fluxes, particularly for N_2O. Similar constraints may apply equally to BRW. In addition to the summertime upwelling of N_2O at THD, there may be also seasonal CFC variations driven by transport of emissions from nearby coastal cities which we cannot rule out.

5.3. Vertical Profiles

[38] Mixing ratio vertical profile anomalies for N_2O and CFC-11 obtained at ETL, Saskatchewan, are shown in Figures 8a–8d. This site was selected as there was a record of monthly aircraft vertical profile measurements from 2006 to 2010, with relatively few missing months. The mixing ratio anomalies are averaged over 2 month periods and plotted against altitude at 1 km intervals. We compare two individual years, namely, 2006, a year with a strong deviation of the jet, and 2008, a year with no significant deceleration of the jet. Figure 8a plots the 2006 N_2O mixing ratio anomalies from winter to summer with a clear distinction between the summer months and the spring and winter (note that vertical profiles were missing in January and October 2006). Mixing ratio anomalies are broadly homogeneous during the summer months, with an apparent increase in the lowermost altitudes during the spring and wintertime periods, possibly reflecting the seasonality of local surfaces fluxes. However, it should be noted that the data are quite noisy with substantial error bars. Summertime N_2O mixing ratio anomalies in 2008 (Figure 8b) are surprisingly similar to the summer and winter months in 2006, again with large uncertainty. Profiles of CFC-11 shown in Figures 8c and 8d are more complicated with much greater variability in their mixing ratio anomalies, with the suggestion that anomalies in 2006 are more homogeneously mixed compared to the summer and winter in 2008. Given the large uncertainties, we accept that this does not allow for a robust interpretation. Figure 8e shows the N_2O mixing ratio anomalies at ULB, Mongolia, during 2006, with a winter-to-summer progression similar to ETL. Even allowing for the uncertainty, they appear to be well mixed over the narrow altitude range. *Ishijima et al.* [2010] reported vertically homogeneous N_2O mixing ratios over Surgut, Siberia, and noted that these vertical profiles will be influenced both by variation in the local-regional fluxes and by the temporal variation of the planetary boundary layer height.

[39] Finally, in Figure 8f, we examine THD N_2O mixing ratio anomalies in July–August 2006 and 2008. Summertime 2006 shows a decrease in mixing ratio over the altitude range, whereas summertime 2008 appears to be more homogeneous. With the large uncertainties, we cannot rule out a contribution from local N_2O coastal upwelling sources in the lowermost altitudes.

6. Relationship With Other Modes of Variation

[40] It is well established that other variations in atmospheric circulation, in particular the El Niño–Southern Oscillation (ENSO) and the North Atlantic Oscillation (NAO), are linked to the strength of the winter stratospheric circulation through dynamical coupling. A positive ENSO and a negative NAO are linked to stronger STE and, thus, deeper summertime minima of the stratospheric tracers [*Calvo et al.*, 2004; *Ineson and Scaife*, 2009]. There is evidence for a significant ENSO signal

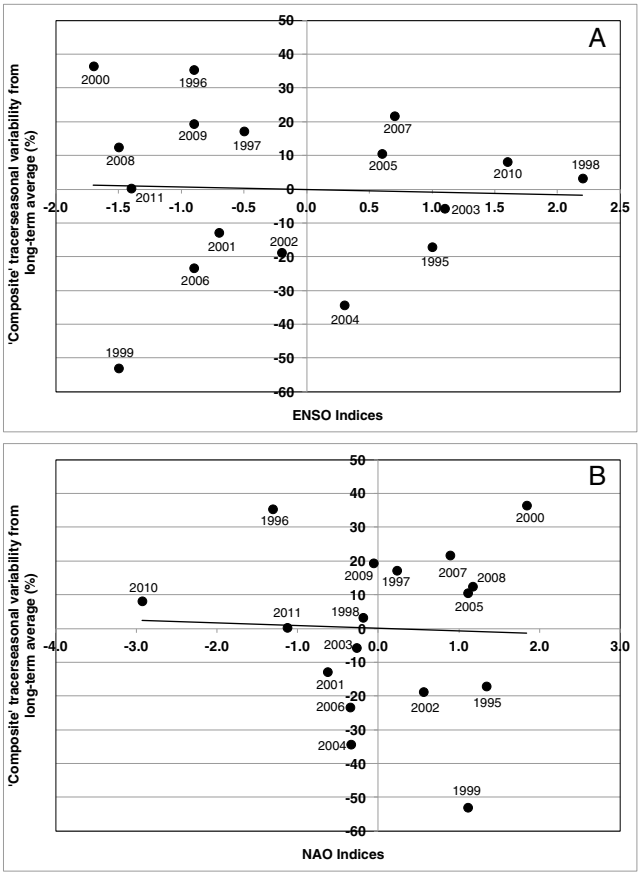

Figure 9. Scatterplots and linear trend line of the seasonal variability component of the MHD composite tracer versus (a) ENSO (ENSO 3.4; www.cpc.ncep.noaa.gov) and (b) NAO [*Hurrell and Deser*, 2009] (www.cgd.ucar.edu/cas/hurrell/indices.html) indices.

in the Arctic stratospheric temperatures [*Manzini*, 2009]. During the intense Arctic stratospheric warming observed in the winter of 2008–2009, *Di Biago et al*. [2010] noted large variability of N_2O, O_3, and CO at Thule (76.5°N, 68.8°W) associated with the rapid transport of air from the extratropics. As discussed by *Hamilton and Fan* [2000], the dynamical quasi-biennial oscillation may modulate STE to produce an additional QBO effect in global mean tropospheric tracer mixing ratios. However, model results for the magnitude of the QBO signal in global mean surface N_2O is estimated to be on the order of 0.1–0.2 ppb yr^{-1} peak to peak [*Hamilton and Fan*, 2000] compared to an average seasonal amplitude of ~0.7 ppb, so the impact of the QBO is likely to be small.

[41] Table 2 lists the Pearson correlation coefficients (r) for each stratospheric tracer at MHD between the mean of the (% deviation from the average) three detrending methods versus the annual NAO [*Hurrell and Deser*, 2009] (www.cgd.ucar.edu/cas/hurrell/indices.html) and ENSO (ENSO 3.4; www.cpc.ncep.noaa.gov) indices. Although N_2O is weakly correlated with ENSO and CFC-11 is also weakly correlated with NAO, these values are not statistically significant. Figure 9 compares the seasonal variability of the composite tracer with the NAO and ENSO indices. The general lack of correlation with these indices suggests that tracer mixing ratios are better correlated with stratospheric winter flow than the major modes of tropospheric variability. This is consistent with the process illustrated schematically in Figure 2.

7. Conclusions

[42] We have demonstrated good correlations between the midstratospheric circulation at 10 hPa, 58–68°N, and the detrended seasonal variability from the baseline monthly mean mixing ratios of the three stratospheric tracers N_2O, CFC-11, and CFC-12. There are several plausible methods for detrending the observed data, and this uncertainty has been included in the analysis by the use of three different methods.

[43] The degree of wintertime (DJF) deceleration of the stratospheric jet is due to enhanced stratospheric wave activity driving the mass transport across the tropopause. With a lag of 3–4 months, this can quantitatively account for much of the interannual variability of the summertime minima of these long-lived trace gases. The year-to-year fluctuations in surface tropospheric mixing ratios of the stratospheric tracers are, as expected, strongly affected by annually varying fluctuations in stratosphere-troposphere mass exchange. As suggested by *Ishijima et al*. [2010], the location of the strongest STE may vary with spatiotemporal distribution of tracers in the stratosphere and the lifetime in the troposphere. The major modes of tropospheric variability, such as the ENSO and the NAO, do not correlate as well with the interannual variability of the seasonal cycles of the tracers.

[44] From the analysis of a very limited number of vertical profiles, we show that these do not contradict our interpretation that STE can result in the transport of depleted mixing ratios of the stratospheric tracers into the lower regions of the troposphere, under conditions when there is strong deceleration of the jet. However, we do recognize that the analysis of a much larger vertical profile database, which was beyond the scope of this study, may potentially provide a more compelling argument.

[45] There are a few years when the relationship between the species' seasonal variability at the surface and the behavior of the jet is broken either collectively or as individual species. In particular, at MHD, we observe an anticorrelation between the composite seasonal variability and the winds after 2008, with BRW also showing anomalous years in 2009 and 2010. Conversely, at THD, the winds and the composite seasonal variability are correlated during 2009–2011. Without more years of observations, we can only speculate on the possible cause of this discrepancy, although we would expect that transient changes in the lower stratosphere distribution of tracers or local/regional emissions coupled to tropospheric transport processes must impact the seasonality of the stratospheric tracers.

8. Potential Applications

[46] It is remarkable that the very small amplitudes (<1%) of the seasonal cycles of these tracers relative to their mean mixing ratios can provide clear evidence of stratospheric circulation and cross-tropopause transport. We can see two potentially novel applications for this work. The first is seasonal forecasting of trace gas values in summer. While seasonal forecasts for many extratropical regions are unreliable and often show low forecast skill [*Arribas et al*., 2011], the link between the previous winter circulation anomalies and the following summer minima in trace gases such as N_2O and CFCs appears to be strong enough to provide potentially high forecast skill for summer variations in trace gases strongly affected by STE, assuming that tracers are not strongly affected by tropospheric factors. The predictor variable of midstratospheric circulation for the winter period is analyzed in near real time by many operational forecast centers [*Swinbank and O'Neill*, 1994]. Given the relationship with the mass flux of tracers entering the troposphere in spring, it would be therefore relatively straightforward to constrain the mixing ratios of these tracers in forecasts or even produce forecasts of the fluctuations, albeit small, in trace gas mixing ratios themselves.

[47] A further novel application of this work is for monitoring the Brewer-Dobson circulation by proxy. This circulation is known to be driven by the same atmospheric wave drag that weakens the strength of the extratropical winter jet in the stratosphere [*Andrews and McIntyre*, 1978; *Holton et al*., 1995]. The average pumping action of the wave drag on the stratospheric meridional overturning results in both the Brewer-Dobson circulation and the relationship between winter stratospheric winds and the transport of tracers from the stratosphere into the troposphere as discussed here. The strength of this relationship gives a year-to-year composite tracer correlation of 0.68 (1995–2011) (Table 1) between the summer minima in the surface mass mixing ratios of the stratospheric trace gases at MHD and the extratropical winter jet. However, it is not possible to directly measure STE and the associated Brewer-Dobson circulation because both the tropical upwelling in the lower stratosphere and the return downwelling flow in the extratropics have small velocities of less than 1 mm/s that are well beyond any direct measurement capability. Trends have so far not been detectable in atmospheric reanalyses [*Iwasaki et al*., 2009] or tracer measurements [*Engel et al*., 2008]. The results shown here suggest an alternative. By detrending the baseline N_2O and CFC-11 and CFC-12 mixing ratios to remove long-term

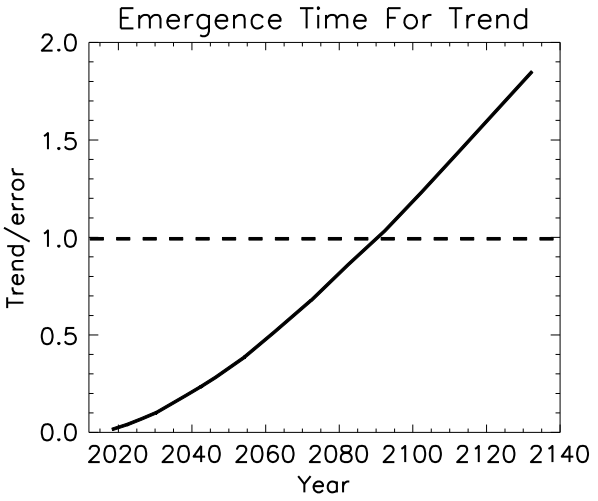

Figure 10. The ratio between the trend in the seasonal cycle of a composite tropospheric tracer and its least squares fit error assuming that future interannual variability in tracer transport remains unchanged. The crossing of the dashed and solid line indicates when the error is equal to the trend so that it starts to become detectable above the natural variability.

variations in global emissions, the depth (peak-to-trough amplitude) of the seasonal cycle can be estimated. Although other processes such as tropopause folds and deep convection may also contribute to stratosphere-troposphere exchange [e.g., *Poulida et al*., 1996; *Fischer et al*., 2003; *Stohl et al*., 2003; *Hegglin et al*., 2004; *Tang et al*., 2011], the residual depth of the summer minimum is so well related to the strength of the Brewer-Dobson circulation that it should be possible to use it as a monitoring tool to test the climate model predictions of increasing the Brewer-Dobson circulation by monitoring the depth of the summer minimum. This depth depends on the difference between summer and winter circulation. However, while the fractional increase is expected to be the same through the seasonal cycle, the difference between summer and winter absolute mass fluxes across the tropopause increases in the future. Climate projection data suggest that the difference in mass flux between winter and summer will increase by around 1.3% per decade [*Butchart and Scaife*, 2001]. Interannual variability in the depth of the summer minimum in our composite tracer is 26%. It is a reasonable assumption that this will remain constant in the future as most climate projections show little change in the interannual variability of the extratropical circulation. We can therefore estimate the uncertainty in any observed trend in the summer tracer minimum and calculate how many years of monitoring would be needed for this trend to be detectable above the climate variability "noise" using standard least squares fitting [*Squires*, 1985]. The results are shown in Figure 10, where it is not until the end of the 21st century that the increasing Brewer-Dobson circulation is likely to be detected in observed tracer mixing ratios. However, if the noise could be attributed to other factors such as ENSO, as described above, and if improved temporal or spatial coverage observations of the tracer species were available, then it may be possible to statistically remove the variability and better estimate the trends in the summer minimum, thereby allowing detection of the trend in the Brewer-Dobson circulation on a shorter time scale.

[48] **Acknowledgments.** We specifically acknowledge the cooperation and efforts of all members of the AGAGE team for their many contributions to the MHD and THD observations, in particular G. Spain for operations at the Mace Head station and P. Salameh for AGAGE software support. We also thank the School of Physics, National University of Ireland, Galway, for making the research facilities at Mace Head available. Unpublished NOAA vertical profile data were provided by B. Miller, C. Sweeney, and S. Montzka, and we thank them for their valuable discussions with respect to these data. We also thank N. Harris and D. Young for valuable discussions and several reviewers who provided constructive comments. The operation of the Mace Head station was supported by the UK Department of Energy and Climate Change (DECC) under contracts GA0201, GA01081, GA01103, and CESA 002; and by the National Aeronautics and Space Administration (NASA grants NAGW-732, NAG1-1805, NAG5-3974, and NAG-12099). The Trinidad Head station and AGAGE network calibrations and data processing are supported by grants from NASA's Upper Atmosphere Research Program. NOAA support comes from the NOAA Climate Program Office under their Atmospheric Chemistry, Carbon Cycle, and Climate (AC4) Program.

References

Andrews, D. G., and M. E. McIntyre (1978), Generalized Eliassen-Palm and Charney-Drazin theorems for waves on axisymmetric mean flows in compressible atmospheres, *J. Atmos. Sci.*, *35*, 175–185.

Arribas, A., et al. (2011), The GloSea4 ensemble prediction system for seasonal forecasting, *Mon. Weather Rev.*, *139*, 1891–1910.

Berrisford, P., D. Dee, K. Fielding, M. Fuentes, P. Kallberg, S. Kobayashi, and S. Uppala (2009), The ERA-Interim Archive, ERA Report Series. 1. Technical Report. European Centre for Medium-Range Weather Forecasts, Shinfield Park, Reading. pp. 16.

Bourqui, M. S. (2004), Stratosphere-troposphere exchange from the Lagrangian perspective: A case study and method sensitivities, *Atmos. Chem. Phys. Discuss.*, *4*, 3249–3284.

Butchart, N., and A. A. Scaife (2001), Removal of chlorofluorocarbons by increased mass exchange between the stratosphere and troposphere in a changing climate, *Nature*, *410*, 799–802.

Butchart, N., A. A. Scaife, M. Bourqui, J. de Grandpré, S. H. E. Hare, J. Kettleborough, U. Langematz, E. Manzini, F. Sassi, and K. Shibata (2006), Simulations of anthropogenic change in the strength of the Brewer-Dobson circulation, *Clim. Dyn.*, *27*, 727–741, doi:10.1007/s00382-006-0162-4.

Calvo, N., R. Garcia-Herrera, R. Garcia, I. Gimeno, P. Ribera, D. Gallego, and E. Hernandez (2004), ENSO signal in the tropical middle atmosphere: Influence of the zonal mean meridional circulation, *Geophys. Res. Abstr.*, *6*, 00,648.

Di Biagio, C., G. Muscari, A. Di Sarra, R. L. de Zafra, P. Eriksen, G. Fiocco, I. Fiorucci, and D. Fuà (2010), Evolution of temperature, O_3, CO, and N_2O profiles during the exceptional 2009 Arctic major stratospheric warming as observed by lidar and millimeter-wave-spectroscopy at Thule (76.5°N, 68.8°W) Greenland, *J. Geophys. Res.*, *115*, D24315, doi:10.1029/2010JD014070.

Douglass, A. R., R. S. Stolarski, M. R. Schoeberl, C. H. Jackman, M. L. Gupta, P. A. Newman, J. E. Nielsen, and E. L. Fleming (2008), Relationship of loss, mean age of air and the distribution of CFCs to stratospheric circulation and implications for atmospheric lifetimes, *J. Geophys. Res.*, *113*, D14309, doi:10.1029/2007JD009575.

Engel, A., et al. (2008), Age of stratospheric air unchanged within uncertainties over the past 30 years, *Nat. Geosci.*, pp. 29–31 doi:10.1038/NGEO388.

Fereday, D., A. Maidens, A. Arribas, A. A. Scaife, and J. R. Knight (2012), Seasonal forecasts of Northern Hemisphere winter 2009/10, *Env. Res. Lett.*, *7*, doi:10.1088/1748-9326/7/3/034031.

Fischer, H., et al. (2003), Deep convective injection of boundary layer air into the lowermost stratosphere at midlatitudes, *Atmos. Chem. Phys.*, *3*, 739–745.

Garcia, R. R., and W. J. Randel (2008), Acceleration of the Brewer-Dobson circulation due to increases in greenhouse gases, *J. Atmos. Sci.*, *65*, 2731–2739, doi:10.1175/2008JAS2712.1.

Garfinkel, C. I., and D. L. Hartmann (2007), Effects of the El Niño–Southern Oscillation and the quasi-biennial oscillation on polar temperatures in the stratosphere, *J. Geophys. Res.*, *112*, D19112, doi:10.1029/2007JD008481.

Hall, B. D., G. S. Dutton, and J. W. Elkins (2007), The NOAA nitrous oxide standard scale for atmospheric observations, *J. Geophys. Res.*, *112*, D09305, doi:10.1029/2006JD007954.

Hall, B. D., G. S. Dutton, D. J. Mondeel, J. D. Nance, M. Rigby, J. H. Butler, F. L. Moore, D. F. Hurst, and J. W. Elkins (2011), Improving measurements of SF6 for the study of atmospheric transport and emissions, *Atmos. Meas. Tech.*, *4*, 2441–2451, 863AS, doi:10.5194/amt-4-2441-2011.

Hamilton, K., and S.-M. Fan (2000), Effects of the stratospheric quasi-biennial oscillation on long-lived greenhouse gases in the troposphere, *J. Geophys. Res.*, *105*, doi:10.1029/2000JD900331.

Hegglin, M. I., et al. (2004), Tracing troposphere-to-stratosphere transport above a mid-latitude deep convective system, *Atmos. Chem. Phys.*, *4*, 741–756.

Holton, J. R., P. H. Haynes, M. E. McIntyre, A. R. Douglass, R. B. Rood, and L. Pfister (1995), Stratosphere-troposphere exchange, *Rev. Geophys.*, *33*, 403–439.

Huang, J., et al. (2008), Estimation of regional emissions of nitrous oxide from 1997 to 2005 using multinetwork measurements, a chemical transport model, and an inverse method, *J. Geophys. Res.*, *113*, D17313, doi:10.1029/2007JD009381.

Hurrell, J. W., and C. Deser (2009), North Atlantic climate variability: The role of the North Atlantic Oscillation, *J. Mar. Syst.*, *78*, 28–41.

Ineson, D., and A. A. Scaife (2009), The role of the stratosphere in the European climate response to El Niño, *Nat. Geosci.*, *2*, 32–36.

Ishijima, K., et al. (2010), Stratospheric influence on the seasonal cycle of nitrous oxide in the troposphere as deduced from aircraft observations and model simulations, *J. Geophys. Res.*, *115*, D20308, doi:10.1029/2009JD013322.

Iwasaki, T., H. Hamada, and K. Miyazaki (2009), Comparisons of Brewer-Dobson circulations diagnosed from reanalyses, *J. Meteorol. Soc. Jpn.*, *87*(6), 997–1006.

Jiang, X., W. L. Ku, R. L. Shia, Q. Li, J. Elkins, R. G. Prinn, and Y. L. Yung (2007), Seasonal cycle of N_2O: Analysis of data, *Global Biogeochem. Cycles*, *21*, GB1006, doi:10.1029/2006GB002691.

Kellmann, S., et al. (2012), Global CFC-11 (CCl_3F) and CFC-12 (CCl_2CF_2) measurements with the Michelson Interferometer for Passive Atmospheric Sounding (MIPAS): Retrieval, climatologies, and trends, *Atmos. Chem. Phys.*, *12*, 18,875.

Liang, Q., R. S. Stolarski, A. R. Douglass, P. A. Newman, and J. E. Nielsen (2008), Evaluation of emissions and transport of CFCs using surface observations and their seasonal cycles and the GEOS CCM simulation with emissions-based forcing, *J. Geophys. Res.*, *113*, D14302, doi:10.1029/2007JD009617.

Liang, Q., A. R. Douglass, B. N. Duncan, R. S. Stolarski, and J. C. Witte (2009), The governing processes and timescales of stratosphere-to-troposphere transport and its contribution to ozone in the Arctic troposphere, *Atmos. Chem. Phys.*, *9*, 3011–3025, doi:10.5194/acp-9-3011-3029.

Liao, T., C. D. Camp, and Y. L. Yung (2004), The seasonal cycle of N_2O, *Geophys. Res. Lett.*, *31*, L17108, doi:10.1029/2004GL020345.

Lueker, T. J., S. J. Walker, M. K. Vollmer, R. F. Keeling, C. D. Nevison, and R. F. Weiss (2003), Coastal upwelling air-sea fluxes revealed in atmospheric observations of O_2/N_2, CO_2 and N_2O, *Geophys. Res. Lett.*, *30*(6), 1292, doi:10.1029/2002GL016615.

Manney, G. L., K. Krüger, J. L. Sabutis, S. A. Sena, and S. Pawson (2005), The remarkable 2003–2004 winter and other recent warm winters in Arctic stratosphere since 1990s, *J. Geophys. Res.*, *110*, D04107, doi:10.1029/2004JD005367.

Manney, G. L., et al. (2008), The evolution of the stratopause during the 2006 major warming: Satellite data and assimilated meteorological analysis, *J. Geophys. Res.*, *113*, D11115, doi:10.1029/2007JD009097.

Manney, G. L., M. J. Schwartz, K. Krüger, M. L. Santee, S. Pawson, J. N. Lee, W. H. Daffer, R. A. Fuller, and N. J. Livesey (2009), Aura Microwave Limb Sounder observations of dynamics and transport during the record-breaking 2009 Arctic stratospheric major warming, *Geophys. Res. Lett.*, *36*, L12815, doi:10.1029/2009GL038586.

Manning, A. J., S. O'Doherty, A. R. Jones, R. G. Derwent, and P. G. Simmonds (2011), Estimating UK methane and nitrous oxide emissions from 1990 to 2007 using an inversion modeling approach, *J. Geophys. Res.*, *116*, D02305, doi:10.1029/2010JD014763.

Manzini, E. (2009), Atmospheric Science: ENSO and the stratosphere, *Nat. Geosci.*, *2*, 749–750.

Mizuta, R. (2012), Intensification of extratropical cyclones associated with the polar jet change in the CMIPS global warming projections, *Geophys. Res. Lett.*, *39*, L19707, doi:10.1029/2012GL053032.

Nevison, C. D., D. E. Kinnison, and R. F. Weiss (2004), Stratospheric influences on the tropospheric seasonal cycles of nitrous oxide and chlorofluorocarbons, *Geophys. Res. Lett.*, *31*, L20103, doi:10.1029/2004GL020398.

Nevison, C. D., N. M. Mahowald, R. F. Weiss, and R. G. Prinn (2007), Interannual and seasonal variability in atmospheric N_2O, *Global Biogeochem. Cycles*, *21*, GB3017, doi:10.1029/2006GB002755.

Nevison, C. D., et al. (2011), Exploring causes of interannual variability in the seasonal cycles of tropospheric nitrous oxide, *Atmos. Chem. Phys.*, *11*, 3713–3730.

Poulida, O., R. R. Dickerson, and A. Heymsfield (1996), Stratosphere-troposphere exchange in a midlatitude mesoscale convective complex, *J. Geophys. Res.*, *101*(D3), 6823–6836.

Prinn, R. G., et al. (2000), A history of chemically and radiatively important gases in air deduced from ALE/GAGE/AGAGE, *J. Geophys. Res.*, *105*, 17,751–17,792.

Rao, S. T., and I. Zurbenko (1994), Detecting and tracking changes in ozone air quality, *J. Air Waste Manage. Assoc.*, *44*, 1089–1095.

Scaife, A. A., N. Butchart, C. D. Warner, and R. Swinbank (2002), Impact of a spectral gravity wave parameterization on the stratosphere in the Met Office Unified Model, *J. Atmos. Sci.*, *59*, 1473–1489.

Squires, G. L. (1985), *Practical Physics*, Cambridge Univ. Press, 3rd Ed., 215 pp., Cambridge CB2 8BS, U.K.

Stohl, A., et al. (2003), Stratosphere-troposphere exchange: A review, and what we have learned from STACCATO, *J. Geophys. Res.*, *108*(D12), 8516, doi:10.1029/2002JD002490.

Swinbank, R., and A. O'Neill (1994), The GloSea4 ensemble prediction system for seasonal forecasting, *Mon. Weather Rev.*, *122*, 686–702.

Tang, Q., M. J. Prather, and J. Hsu (2011), Stratosphere-troposphere exchange ozone flux related to deep convection, *Geophys. Res. Lett.*, *38*, L03806, doi:10.1029/2010GL046039.

Taws, S. L., R. Marsh, N. C. Wells, and J. Hirschi (2011), Re-emerging ocean temperature anomalies in late 2010 associated with a repeat NAO, *Geophys. Res. Lett.*, *38*, L20601, doi:10.1029/2011GL048978.

Wernli, H., and M. Bourqui (2002), A Lagrangian "1-year climatology" of (deep) cross tropopause exchange in the extratropical Northern Hemisphere, *J. Geophys. Res.*, *107*(D2), 4021 doi:10.1029/2001JD000812.